The elastoplastic behavior of yield stress fluids

Élie Merveille N'Gouamba, Julie Goyon, Philippe Coussot

The elastoplastic behavior of yield stress fluids

E. N'Gouamba, J. Goyon, P. Coussot

Univ. Paris-Est, Laboratoire Navier (ENPC-IFSTTAR-CNRS), 77420 Champs sur Marne, France

Abstract: By means of the incremental elastic modulus for small deformations superimposed on creep and subsequent recovery tests, we follow the structural state of various soft-jammed systems (yield stress fluids) in their solid regime. We demonstrate that the solid state of the material is associated with a persistent elastic network of constant elastic modulus up to yielding (solid-liquid transition), while progressively more additional elastoplastic elements are involved. The main features of these elastoplastic elements, i.e. increase of both the plastic and the elastic deformation components with the square of the shear stress, reveal the fundamental characteristics of a simple generic model (independent of material structure) describing the different components of the mechanical behavior of such systems in their solid regime.

1. Introduction

A wide range of materials (emulsions, gels, foams, colloids, etc) are soft-jammed systems, deforming only in a finite way below some critical stress, but flowing indefinitely, like liquids, beyond this stress. These trends have long been identified as the hallmark of yield stress fluids [1-2] and were at the origin of the idea that these systems might be considered as analogous to glasses by replacing the temperature by the stress [3-4].

As apparently described by a generic phenomenological model, i.e. the so-called Herschel-Bulkley model [5-7], the mechanical behavior of these systems in the liquid regime has attracted so far the most attention by physicists [8-12] who have proposed models for the physical origin of this behavior and the parameters of this model. On the other side, the solid regime behavior, and in particular the elastic components, appear to play a significant role under various flow conditions [13]. Nevertheless, theoretical approaches for the basic aspects of the behavior in this regime, i.e. the stress vs deformation relationship, have been proposed [14-18], but these models are essentially aimed at good prediction of the transitional characteristics, i.e. the characteristics of the solid to liquid transition, and the proposed behavior in the solid regime is generally rather simplistic. So far, the mechanical response in the solid regime has essentially been considered in details through its dynamical aspects: creep flow [19-21], aging [19, 22-24], characterization of the solid/liquid transition [22]. The detailed components of the constitutive equation for the static regime have not been explored experimentally, and it is a fortiori not yet clear whether there exists some generic behavior in this regime.

Yet, the solid regime is of wide interest, not only as its complete description might provide keys for understanding or predicting the solid-liquid transition, but also because of the analogy of these systems with amorphous materials such as metals and glasses or plastic materials [7] and the research on the physical origin of plasticity. It was in particular shown, generally by means of simulations, that plastic deformation manifests as local rearrangements exhibiting a broad distribution of sizes and shapes [25-26], non-affine displacements [27], and connectivity changes between particles [28] that lead to a redistribution of elastic stresses in the system [29]. Furthermore, the collective behavior of these reorganizations includes spontaneous strain localization, intermittent dynamics, power-law distributed avalanches [30] and spatial cooperativity [31]. On the experimental side, diffusion-wave spectroscopy also directly provided information about reversible and irreversible motions as a function of deformations [32-33] and direct 3D-imaging of the structure evolution finally showed localized irreversible shear transformation zones [34] and growing clusters of non-affine deformation percolating at yielding [35]. However, the relationship between these rearrangements and the

mechanical behavior has been rarely explored. The standard rheological approaches such as the frequency sweep basically developed for polymers, the strain or stress amplitude sweep to appreciate the solid-liquid transition [5], or even more sophisticated ones such as LAOS [17, 36], do not provide clear information on this question. Here we propose a new probing of the structure, which provides both a new way for appreciating plastic and elastic events (through their impact on macroscopic deformation) and detailed information on the mechanical behavior.

We follow the structural state of various soft-jammed systems by means of their elastic modulus at small deformation and recovery tests after different deformations in the solid regime. This makes it possible to show that the solid regime is characterized by the persistence of a network of constant elastic modulus over the whole range of deformations, with additional elastic and plastic deformations of similar value and increasing with the square of the applied stress. From this information we deduce a detailed and generic mechanical description of the behavior of jammed systems in their solid regime.

2. Materials and procedures

We test a set of materials with various types of structures: an oil in water emulsion, a physical gel (Carbopol), a model colloidal suspension (laponite), and a natural clay water system (bentonite).

2.1 Materials

A concentrated direct (oil in water) emulsion (volume fraction: 87%) was prepared by dispersing Dodecane (oil) in a mixture of water and 3 wt % of TTAB (tetradecyltrimethylammonium bromide), an ionic surfactant. Dodecane is progressively poured in the water-surfactant solution and dispersed as droplets by using a *Silverson* mixer (model L4RT). The velocity of the mixer is increased in steps of 500 rpm up to the maximum velocity (6000 rpm). This process leads to a homogeneous emulsion with a rather well controlled droplet size ($\approx 2\ \mu m$) [40]. The high volume fraction of oil droplets form a compact network which has to be broken for flow to occur.

We use a commercial hair gel from *Couleur Soleil*. This is a Carbopol gel which mainly contains carbomers (Polyacrylic acid), which release H^+ ions, dispersed in water and a concentrated base in order to neutralize the solution. The polymers then organize in spherical structures which swell until reaching a jammed state. The material may be seen as a soft glass comprised of individual elastic micro-sponges of size depending on the preparation and generally in the range $1-10\,\mu\mathrm{m}$ [41-42].

We used Laponite, a synthetic hectorite clay, from *Atlantis Stouls CXD-France*, to prepare a 2.5 wt % aqueous suspension. The powder is poured into water and mixed with a magnetic stirrer during 20 min, which gives a macroscopic homogeneous liquid with a viscosity quite similar to water. Afterwards, salt (NaCl) is added at a concentration of $5x10^{-3}$ mol/l and the suspension is thoroughly mixed with a paddle stirrer at 2000 rpm during 20 min, then left at rest for two weeks. Laponite particles are disk-shaped particles with a thickness of 1 nm and a diameter of 25 nm. They are negatively charged at their faces, and positively at their edges. There is no consensus about the association mode [43] of these platelets (aggregation face/face, association edge/face or association edge/edge…). However the main point is that, since the particles charges are screened by Na^+ ions, their oppositely charged surfaces can be linked by weak Van der Waals forces to form a network spanning the sample at rest, at the origin of their yield stress [44].

Bentonite is an absorbent aluminium phyllosilicate clay consisting mostly of montmorillonite. We used a bentonite *C clair T* from *Mon-Droguiste.com* to prepare a 12 wt % of aqueous suspension. Dry bentonite powder is poured into distilled water and mixed thoroughly with a paddle stirrer at 2000 rpm during 25 min. The suspension is then left at rest for one week to hydrate clay particles. Bentonite particles are long flexible platelets of large aspect ratios, with a thickness around $10\ \mathrm{nm}$ and a length around $1\ \mu\mathrm{m}$ [45]. It has been suggested that they form a lenticular network resulting from random aggregation of these flexible platelets, thus exhibiting an alternation of dense clay-water regions and

water pores with a size of the order of the particle length [46-47]. This type of material is a typical thixotropic fluid, i.e. whose rheological behaviour at a given time depends on the flow history.

All these materials are yield stress fluids, i.e. they are able to flow steadily only when a stress larger than a critical stress (i.e. τ_c, the yield stress) is applied. Concentrated emulsions and Carbopol gels are known to be essentially simple yield stress fluids [48-50], whereas laponite and bentonite suspensions are thixotropic yield stress fluids, i.e. their apparent yield stress increases with the time of rest before the test and their apparent viscosity decreases in time during flow [51-53]. A detailed characterization of these features is out of the scope of the present work which will focus on the material properties in the solid regime of these fluids.

2.2 Rheometry

For these tests we used a controlled stress Malvern Kinexus rheometer equipped with rough (to avoid wall slip) parallel disks (50 mm diameter) and a gap of 1 mm. The resolution on the rotation angle measurement is 10 nrad, which gives a deformation resolution of 2.5×10^{-7}. Note that for long tests we place a wet system around the sample periphery to damp evaporation.

We carried out creep tests consisting in imposing a given shear stress (τ) to the material initially at rest and follow its deformation in time. Recovery tests were also carried out after some time of creep, which consisted to abruptly release the stress and follow again the deformation in time.

Since bentonite and laponite suspensions are thixotropic materials their mechanical characteristics (e.g. elastic modulus and yield stress) vary with time. Thus, to perform creep tests with such materials, a reference state should be defined prior to any measurement. Here, the reference state is obtained by first pre-shearing the material at a high shear rate ($150\,\mathrm{s}^{-1}$ for bentonite and $500\,\mathrm{s}^{-1}$ for laponite) during 1 min to erase their flow history (rejuvenation), then leaving the material at rest during 1 min. From this reference state, we apply a stress and follow the deformation as a function of time and then repeat the entire procedure at other stress levels, to have the same reference state.

The emulsion and Carbopol gel are simple yield stress fluids but, after some flow, there can remain some residual stress progressively relaxing. This appears to negligibly affect yield stress or elastic modulus measurements, but this might slightly affect the deformation in the solid regime. To avoid such problem, we also prepare the material in a reference state before each (creep) test, by pre-shearing it during a short time (10 s) at a shear rate of $100\,\mathrm{s}^{-1}$ then leaving it at rest for 1 min.

In order to probe the structure of the different materials during creep tests in the solid regime ($\tau < \tau_c$), we also use a more original but robust test [22] which consists in superimposing to a constant stress (τ_0), a small stress oscillation, so that the total stress writes $\tau = \tau_0 + \varepsilon \sin \omega t$, with ω the frequency of the oscillations. The frequency is kept constant at 1Hz, results are generally independent of the frequency for such materials [54]. The resulting deformation can be well represented as $\gamma = \gamma_0 + \eta \sin(\omega t - \varphi)$, in which γ_0 and η are deformation amplitudes and φ the phase shift. Here the amplitude of the oscillations (ε) is chosen so as to induce an additional deformation in the linear regime of the materials. The typical value resulting from this choice for ε was 10^{-3}. An "elastic" (G') and a "viscous" (G'') moduli associated with the material behaviour under such oscillations are then computed as $G' = (\varepsilon \cos\varphi)/\eta$ and $G'' = (\varepsilon \sin\varphi)/\eta$.

3. Results and discussion

3.1 Constant elastic network before yielding

The different flow regimes of these materials appear from a simple procedure which consists to apply a shear stress (τ) to the material and follow the resulting deformation (γ) as a function of time (t).

The test is then repeated at another stress level, with the material prepared in the same initial state (e.g. preshear then resting time).

Under such conditions we typically observe two distinct regimes for all the yield stress fluids (see inset of Fig.1, and Appendix 1 for the other materials): for τ smaller than a critical value (i.e. the material yield stress, τ_c) the material is just slightly deformed over a short time, then γ reaches a plateau indicating that no further significant motion occurs (and if there is some slow flow the apparent shear rate continuously decreases towards zero); for $\tau > \tau_c$, after a short period, γ increases linearly with time, indicating that the material flows steadily. In that case we can define $\dot{\gamma}$, i.e. the apparent steady state shear rate associated to τ , as the slope of the $\gamma(t)$ curve. This makes it possible to distinguish the solid regime, associated with negligible flow and limited deformation, from the liquid regime, associated with steady-state flow after some time. For simple yield stress fluids we get values for $\dot{\gamma}$ going down to low values when $\tau \to \tau_c^+$.

For thixotropic yield stress fluids (laponite and bentonite) there exists a finite value (i.e. a critical shear rate) below which we cannot get a steady state flow [55]. This clearly appears from the fact that in Figures A2a and A2b, at the solid-liquid transition, there is a large gap between the two sets of the deformation vs time curves corresponding respectively to the solid and the liquid regime, because the shear rate jumps to a relatively large value when the applied stress is slightly increased above the yield stress. However this trend will not play a significant role here, since we focus on the solid regime characteristics.

On another side, for some materials, γ goes on slightly increasing in time for $\tau < \tau_c$, and $\dot{\gamma}$ continuously decreases in time (see e.g. Figure A3). We will leave apart such creep flows corresponding to viscous and/or aging effects in the solid regime and, by means appropriate experimental protocols (see below), we will focus on (instantaneous) elastoplastic effects observed through the deformation induced over short times.

In order to probe the structure during the deformations induced in these creep tests we superimpose small oscillations and measure the corresponding elastic and loss moduli of the material, as defined above. Remarkably, in the solid regime, after a short transient period, the elastic modulus keeps a high value and remains constant, even for $\tau \to \tau_c$ (see Fig. 1). This means that whatever the (total) deformation undergone by the system, there persists a similar elastic network. Similar conclusions were previously reached by measuring the elastic modulus from the analysis of the elasto-inertia oscillations during start up flow [56]. Note that this technique induces uncontrolled small amplitude oscillations.

This result, i.e. the constancy, under small deformation, of the elastic modulus in the solid regime, appears to be valid for any type of soft-jammed system (see Fig. 2). We can nevertheless remark that for the clay suspension (bentonite) some slight increase of this modulus can be observed, suggesting that there is in addition a strain hardening effect for larger deformation tending to reinforce this basic elastic network, a trend that we will neglect in the following.

Since this elastic network, observed under small oscillatory deformations, persists at any (constant) deformation in the solid regime, this means that it constitutes a fundamental component of the structure of the material whatever the deformation in this regime.

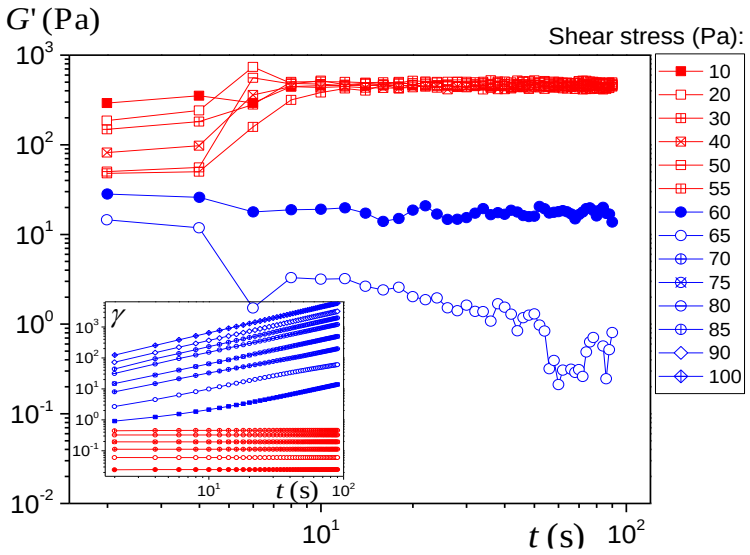

Figure 1: Elastic modulus of the emulsion measured from oscillations under low stress amplitude as a function of time during creep tests under various shear stress values (see legend). The red square symbols correspond to the solid regime ($\tau < \tau_c$), the blue circle symbols correspond to the liquid regime ($\tau > \tau_c$). The inset shows the corresponding deformation undergone by the fluid in time (same symbols).

Just beyond τ_c, the elastic modulus collapses, it typically drops of several orders of magnitude (see Fig.2). Thus, the elastic structure prevailing in the solid regime appears to be fully broken. However, since in that case the material flows and is thus widely deformed (see inset of Fig.1) while we impose additional low stress oscillations, this measure cannot be considered as reflecting the properties of some fixed network or structure, since the structure evolves continuously in time, at a rate. In this context, the meaning of the G' measure is unclear. Here, the main point is that G' is constant all along the solid regime, i.e. up to this transition point.

In parallel, the loss modulus (G''), does not vary much below the yield stress (see inset of Fig.2), and remains much lower than the elastic modulus in the solid regime for all materials (see Fig.2). Beyond the yield stress, for simple yield stress fluids (emulsion and gel), G'' suddenly jumps at a higher value, then progressively decreases towards low values when τ increases (see Fig.2 inset). For thixotropic fluids, it drops to much lower values just beyond the yield stress and keeps close values as the stress increases.

Actually, these variations for $\tau > \tau_c$ can find a simple explanation. The material behavior in its liquid state may be well described by a Herschel-Bulkley model, i.e. $\tau = \tau_c + k\dot{\gamma}^n$, with k and n two material parameters (see Appendix 3). For a creep flow under given stress plus a small oscillating stress the shear rate is given by $\dot{\gamma} = \dot{\gamma}_0 + \eta\omega\cos(\omega t - \varphi)$ and must satisfy $\tau = \tau_0 + \varepsilon \sin \omega t = \tau_c + k\dot{\gamma}^n$. It follows that for stationary oscillations, at first order, $\tau_0 = \tau_c + k\dot{\gamma}_0{}^n$, $\varphi = \pi/2$, $G' = 0$ and $G'' = \varepsilon/\eta = n\omega(\tau_0 - \tau_c)/\dot{\gamma}_0$.

The agreement of this prediction with the data is excellent for the simple yield stress fluids, except just beyond the yield stress for the gel (see Fig.2). This discrepancy may be due to some elastic effects or to some flow heterogeneity around the yield stress values, as already observed for this material type [19]. For the thixotropic fluids, this theoretical approach effectively predicts the negligible observed values for G', and the low and almost constant values for G'' (see inset of Fig.2). Note however that

the exact level and shape of the G'' variations are not well predicted, which may be due to the very low, and thus uncertain, values observed in this regime.

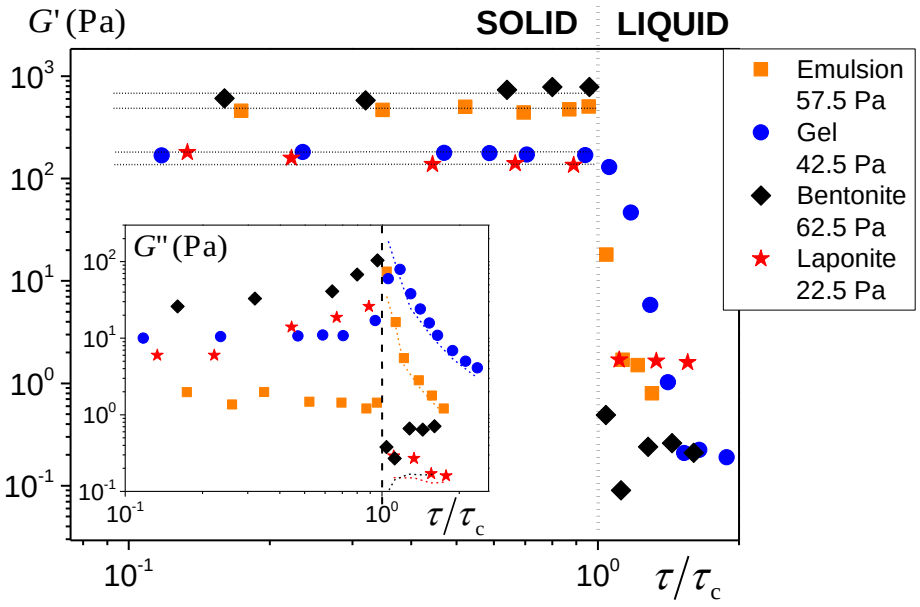

Figure 2: Elastic modulus for low oscillations during creep tests as a function of the imposed shear stress value rescaled by the yield stress, for different materials: emulsion (orange squares), Carbopol gel (blue circles), laponite suspension (red stars), bentonite suspension (black diamonds). The legend gives the material yield stress values. The horizontal dotted lines indicate the (mean) value (G_∞) retained for the elastic modulus in the solid regime for each material. The inset shows the loss modulus measured during the same creep tests by means of small oscillations (same symbols). The dashed lines in the inset correspond to the calculated G'' values at first order according to theory (see text). Note that for laponite and bentonite the moduli values are taken 20 s after the test beginning, i.e. before the significant evolutions observed later during the flow (see Appendix 1).

3.2 Elastic and plastic components

We now turn to a further analysis of the behavior in the solid regime. In that aim, after a creep test under constant stress, we release the stress and observe the deformation in time. This deformation typically rapidly decreases towards a plateau (see Fig.3 inset). The oscillations observed at short time (before 0.5 s) both at the very beginning of the creep test and in the very first times of the recovery test (see inset of Fig.3), are due to the coupling of the material elasticity with the system inertia. These oscillations soon damp and the deformation stabilizes at some level. The elastic component (γ_e) of the deformed solid structure then corresponds to the recovered deformation (difference between the initial value and the deformation plateau), while the plastic component (γ_p) is the non-recovered deformation (see inset of Fig.3).

Note that for this analysis we wish to focus strictly on elastic and plastic effects and leave apart the possible viscous and/or aging effects inducing some slow flows. However, during creep tests, except for the emulsion, in the solid regime the deformation does not strictly reach a plateau, i.e. there is some slight creep flow (See Appendix 2, Figure A4a), which results from such viscous and/or aging effects. In order to leave apart these effects and estimate the deformation resulting from “immediate” elastic or plastic effects only, we reduce the duration of creep tests to have deformation data (see

Figure A4a) over short times (typically less than 3 s). We then take the immediate deformation as the level of the plateau around which elasto-inertia oscillations occur in the initial phase (see [19]). We then release the stress at a time as close as possible to the end of the oscillating period, again in order to avoid viscous effects before recovery. Again some oscillations can be observed in the very first times of the recovery, and we take the deformation recovery as that observed in the plateau just after the end of oscillations (Figure A4b).

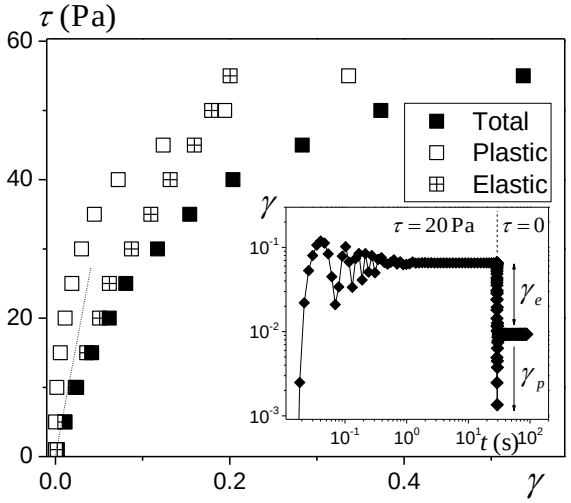

Figure 3: Shear stress vs induced deformation during recovery tests (stress release) for the emulsion: elastic (reversible) component (crossed squares), plastic (irreversible) component (open squares), total deformation (filled squares). The dotted line is the equation $\tau = G_\infty \gamma$, with G_∞ taken as the constant G' (490 Pa for the emulsion) in small oscillations tests. The inset shows a typical recovery test: deformation induced during creep test then deformation recovery for stress release, allowing to distinguish the two (elastic and plastic) components.

For all the materials γ_e and γ_p increase non-linearly with τ (see Fig.3). This increase of γ_p, starting from low stress values, is consistent with the observation of an increasing volume fraction of irreversible rearrangements with the strain amplitude in emulsions [32].

On the other side, the increase of γ_e with τ might be viewed as a consequence of an elastic network with non-linear characteristics. However, the simultaneous increase of γ_p with τ suggests another common physical origin: the progressive implication, in the deformation, of structure components exhibiting an elasto-plastic behavior, in addition to the elastic deformation associated with the basic elastic network distinguished above (of elastic modulus called G_∞ in the following). In order to check this assumption, for each stress value, we subtract, from the total elastic component, the deformation (i.e. τ/G_∞) of the constant linear elastic network submitted to this stress: $\Delta\gamma_e = \gamma_e - \tau/G_\infty$. Note that for very low stress we expect a linear regime, which should lead to $\gamma_e \approx \tau/G_\infty$, as in this linear regime the shear modulus should be equal to the constant elastic modulus from smaller oscillations. As may be seen in Figure 3, Figure A1c, A2c and A3, for a stress much smaller than the yield stress (typically 1 Pa in our measurements) we effectively have an excellent agreement between the apparent shear modulus associated with elastic deformation under creep tests and the deformation predicted from G_∞ determined from the superimposition of small oscillations (values associated with the plateau in Fig.2). The total elastic deformation then rapidly deviates from the simple straight line $\gamma_e \approx \tau/G_\infty$ (see e.g. Fig.A1c).

We then compare the resulting (additional) elastic component ($\Delta\gamma_e$) to the plastic component: it appears that they are very close over the whole range of stresses (typically covering one decade and half) (see Fig.4) except, in some cases, at the approach of τ_c. Moreover, these components vary with the square of the stress (see Fig.4). This result supports the idea of additional elasticity and plasticity progressively involved as τ increases, and with a specific link between the two components.

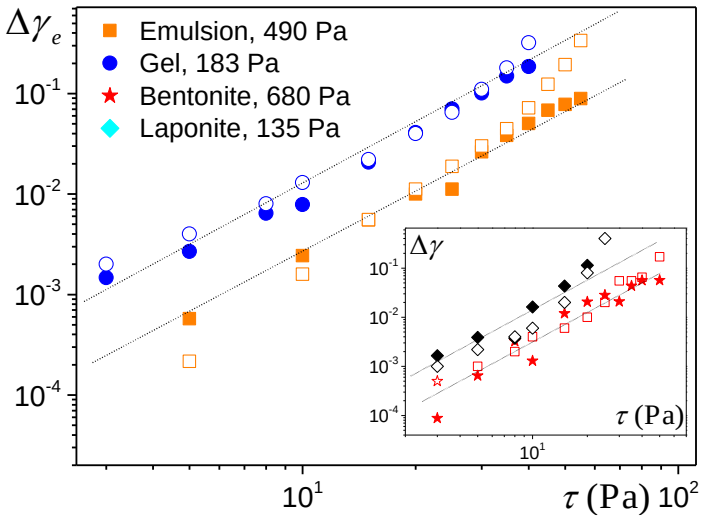

Figure 4: Additional elastic deformation (filled symbols) with regards to the deformation of the constant elastic network, and plastic deformation (open symbols), as a function of the stress applied for different materials (same type of data in the inset). The dotted lines (of slope 2) corresponds to the model fitted to data (see text) with $\alpha = 0.8$ (emulsion), $\alpha = 1$ (gel), $\alpha = 0.5$ (colloid (laponite)), $\alpha = 1.2$ (clay (bentonite)).

4. Modelling

These observations allow us to build a model representing the mechanical behavior in the solid regime. The persistence of an elastic network of constant elastic modulus whatever the deformation, imposes a representation with a basic spring of modulus G_∞ in series with a solid remaining perfectly rigid under low stress but also able to store some elastic energy under some conditions. Thus we expect that this additional solid will be made of elasto-plastic elements. These additional elements cannot involve simple elastic elements in series with other elasto-plastic elements, otherwise the elastic modulus of the whole system would differ from G_∞. These elements should thus basically include some spring (of elastic modulus, G) in parallel with a frictional slider (with a yield value, $\sigma < \tau_c$). Note also that here we definitely focus on the solid regime, and not on the liquid regime or the transition to the liquid regime. This in particular means that the model does not need to predict by itself the transition to the liquid regime, it will be sufficient to consider, besides, that the liquid regime is reached for an applied stress $\tau > \tau_c$.

Let us assume that there is only one such elasto-plastic element, in addition to the basic constant elastic network, as represented in Figure 5. This predicts a purely elastic deformation, $\gamma = \tau/G_\infty$, for an applied stress $\tau < \sigma$, as in that case the slider precludes the deformation of the second element. A deformation involving an elastic and a plastic components, i.e. $\gamma = \tau/G_\infty + (\tau - \sigma)/G$, is nevertheless obtained for $\sigma < \tau < \tau_c$, as the stress on the second element is now sufficient to decompose as a term (σ) associated with the slider motion and a term allowing spring stretching ($\tau - \sigma$). In this case, when

the stress is released, the deformation of the first (purely elastic) element is entirely recovered, while the deformation of the second element is recovered partially only if the stress associated with spring deformation allows to move the slider oppositely. More precisely, the non-recovered (plastic) deformation is $(\tau-\sigma)/G$ for $\tau<2\sigma$, and σ/G for $\tau_c>\tau>2\sigma$. This model globally reproduces the trends observed for the different materials (see e.g. Figure 3): the elastic and plastic components both grow with the imposed stress (see Fig.5). However, in details, this does not fit to our observations which show that: (i) a plastic component appears at low stress, (ii) this component does not increase linearly with the applied stress and (iii) is not constant beyond some point (see Figs. 4 and 5).

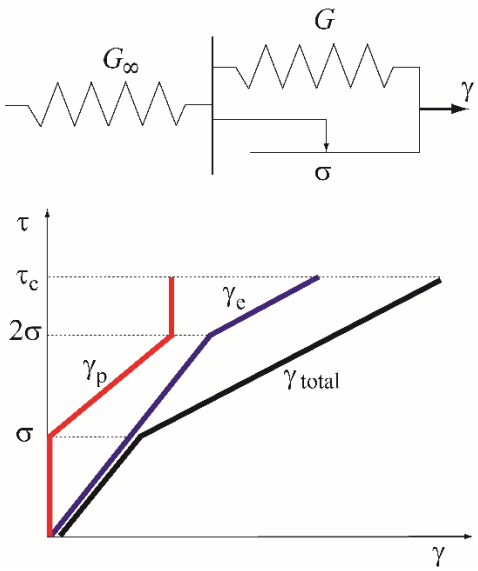

Figure 5: (a) Representation of the simplest model reproducing the constant elastic network and some additional elastoplastic component. (b) Resulting elastic, plastic and total deformation components when submitted to stress then recovery, for different stress levels.

In order to build a model which will be able to represent these different trends (i.e. (i), (ii) and (iii)), we suggest to extend the above behavior type, in the form of a series of such basic elements of critical stress $\sigma_{1,2,\ldots n}$ and elastic modulus $G_{1,2,\ldots n}$ (see Figure 6).

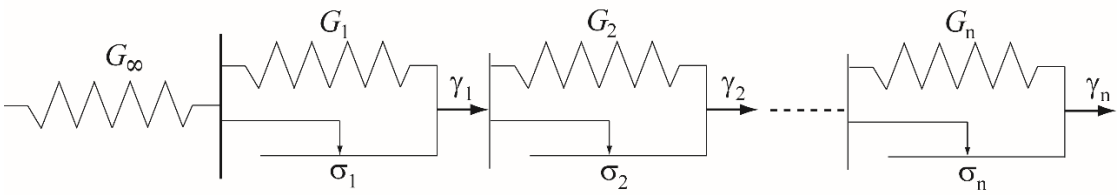

Figure 6: Representation of the complete model (see text) in discrete form.

A continuous version of this model assumes a series of elements of critical stress σ and elastic modulus $G(\sigma)$, with σ ranging from 0 to τ_c, in agreement with our observations. Moreover the weight of each of these elements is described by the density distribution $n(\sigma)$ of such elements over the range $[0-\tau_c]$, so that the number of elements with a critical stress between σ and $\sigma+d\sigma$ is $nd\sigma$. In this context, the model is completely described by the two functions $G(\sigma)$ and $n(\sigma)$.

Under these conditions, the deformation undergone by the material (initially fully relaxed) when a stress τ is applied is:

$$\gamma = \frac{\tau}{G_\infty} + \int_0^\tau \frac{(\tau - \sigma)}{G} n d\sigma \quad (1)$$

When this stress is released, the elements for which $\sigma > \tau/2$ will not recover at all, and the other elements will partially recover down to a residual deformation σ/G. Finally the plastic deformation is

$$\gamma_p = \int_0^{\tau/2} \frac{\sigma}{G} n d\sigma + \int_{\tau/2}^\tau \frac{\tau - \sigma}{G} n d\sigma \quad (2)$$

and the elastic recovery is

$$\gamma_e = \gamma - \gamma_p = \frac{\tau}{G_\infty} + \int_0^{\tau/2} \frac{(\tau - 2\sigma)}{G} n d\sigma \quad (3)$$

Equations (2) and (3) describe the detailed mechanical behavior (when a given stress is applied) within the frame of this very general model.

Let us now examine the implications of the experimental observations on the parameters of this model.

If we impose that the expression (2) for γ_p varies with τ^2, we deduce by derivation that $\int_{\tau/2}^\tau (n/G) d\sigma \propto \tau$, which implies that n/G is constant. A similar conclusion is reached if we assume instead that $\Delta\gamma_e \propto \tau^2$. Now, with n/G being constant, it follows from (2) and (3) that $\Delta\gamma_e = \gamma_p$.

If, instead of assuming the square variation of the plastic deformation with the stress, we initially only assume that $\Delta\gamma_e = \gamma_p$, a derivation of this equation using (2) and (3) leads to $d(\gamma_e - \tau/G_\infty)/d\tau = d\gamma_p/d\tau$, from which we deduce : $\int_0^\tau \frac{n}{G} d\sigma = 2\int_0^{\tau/2} \frac{n}{G} d\sigma$. Since a function such that $f(2\tau) = 2f(\tau)$ is linear, we deduce that $\int_0^\tau \frac{n}{G} d\sigma \propto \tau$, which means that n/G is constant, from which we deduce the square variation of the deformation with the stress.

It is thus remarkable that each of the main features of the variations of the elastic and plastic components identified experimentally has, independently, within the frame of this general model, the same implication on the variation of n/G. This demonstrates the consistency and robustness of these characteristics with regards to this modelling approach.

Besides, note that this model effectively predicts that, when imposing an oscillation of small amplitude ε around a much larger stress τ_0, the apparent elastic modulus is equal to G_∞ whatever the stress value and the resulting total deformation. Indeed, in that case only the (additional) elements for which $\sigma < \varepsilon$ can recover, which corresponds to a fraction of elements $n\varepsilon$, undergoing a deformation recovery $2(\varepsilon - \sigma)/G$. The resulting total deformation recovery of the additional elements will thus be of order ε^2, negligible compared to the recovery of the basic elastic network which is of the order ε.

We can now finalize the fitting of this model to our data. Actually, it is natural to simply assume that G is constant and equal to G_∞ which, as a macroscopic parameter, represents some average of the elastic properties at the local (particle) scale, and thus should also well represent the elastic properties of other kinds of events in the medium. This assumption on the elastic modulus implies that n is constant, which means that the distribution of the different additional elastoplastic events is uniform over the possible range of stresses. This may be written $n = 4\alpha/\tau_c$ with α a parameter to be

determined (from experimental data), which reflects the total amount of elastoplastic elements in the material, since $\alpha = 1/4 \int_0^{\tau_c} n d\sigma$.

From (2) and (3) we deduce the different deformation components observed when a given stress is applied:

$$\gamma_p = \alpha \frac{\tau^2}{G_\infty \tau_c};\ \gamma_e = \frac{\tau}{G_\infty} + \alpha \frac{\tau^2}{G_\infty \tau_c}\ ;\ \gamma = \frac{\tau}{G_\infty} + \frac{2\alpha\tau^2}{G_\infty \tau_c} \quad (4)$$

Since it has been built in relation with the main experimental features, we obviously have a good agreement of this model with the data (see Fig.4). The fit of this model to the data (see Fig.4) surprisingly gives values for α in a rather narrow range, i.e. between 0.5 and 1.2. This means that despite the various microstructures of these materials, made of polymer blobs, droplets, platelet particles or long deformable sheets, not only the mechanical properties in the solid regime have similar features and can be described with a single model, but also the physical details, such as the density of elastoplatic events, are close from each other.

Finally, according to this model, the critical deformation is $\gamma_c = (2\alpha + 1)\tau_c / G_\infty$. For the emulsion this actually does not exactly correspond to the effective value, due to the faster increase than the square stress function of the plastic component at the approach of the yield stress (see Fig.4). For the other materials this represents a good prediction of the observed value, as expected by construction of the model. At last, remark that this model clarifies the question of a linear regime at small deformation: such a regime may be observed when the second (non-linear) term of the total deformation (last equation of (4)) is small compared to the first term, i.e. $\tau << \tau_c / 2\alpha$.

5. Conclusion

By looking at the detailed mechanical characteristics of soft jammed systems we were able to demonstrate that the solid state of these materials is associated with a persistent elastic network of constant elastic modulus up to yielding, while progressively more additional elastoplastic elements are involved. A simple generic model describing the main features of these elastoplastic elements, i.e. similar increase of both the plastic and the elastic deformation components with the square of the shear stress, has been proposed.

The strength of this approach is that it is entirely deductive, i.e. the structure of the model has been established thanks to the main experimental observations. This model seems compatible with the elasto-plastic models [7] generally used for amorphous systems which predicts elastoplastic events of larger amplitude as the stress increases, and with the observation of the growing size of non-affine structures with increasing deformation in colloidal systems [35].

Our approach finally establishes a generic model of the mechanical behavior of soft-jammed systems in their solid regime, which might provide key elements concerning the physical origin of this behavior. Indeed, it is interesting to see that despite relatively complex phenomena when looking at the structure characteristics, the impact in terms of stresses vs deformation is rather simple. Considering that this model applies to soft materials independently of their structures, this suggests that it is inherent to a solid structure and thus might be applicable to standard solids too.

The fact that such a generic model applies to a set of materials of such various structures, suggests that the fundamentals of this model rely on the common property of these materials, i.e. their jammed structure, whatever the physico-chemical origin of the interactions leading to this jamming. Let us for example consider an emulsion. The mechanical behavior may be related to the existence of a constant network of (repulsive) interactions throughout the sample, which is at the origin of the constant elastic modulus for small deformations. This network persists whatever the deformations undergone by the

system in the solid regime, i.e. the initial structure is not broken yet. This structure is nevertheless disordered, so that the droplets are locally jammed, and thus in potential wells, but the depth of these wells lies in a wide range; for example, it seems possible that some droplets can be moved out of their potential well thanks to some slight force leading to a very small displacement, while others can be moved out only thanks to a local stress approaching the yield stress. For some deformation, a fraction of these droplets would thus be removed from their potential well leading to some plastic deformation, affecting the global network but leaving its elastic modulus (for small deformation) unchanged. Such a scheme may be extended to other disordered jammed materials, the condition being that a sufficient disorder exists in the structure which leads to a wide distribution of potential wells. The square variation of the plastic component with the stress results from this distribution, but it remains to be found why such a generic distribution exists in these systems.

Acknowledgements: We acknowledge the support of the French National Research Agency within the frame of the grant ANR-17-CE05-0023-04. We are grateful to Guillaume Ovarlez for his valuable comments on a preliminary version of this work.

References

[1] E.C. Bingham, *Fluidity and Plasticity* (McGraw Hill, New York, 1922)

[2] P. Coussot, Bingham's heritage, Rheol. Acta, 56, 163 (2017)

[3] A.J. Liu, S.R. Nagel, Jamming is not just cool any more, Nature, 396, 21 (1998)

[4] M.E. Cates, J.P. Wittmer, J.P. Bouchaud, P. Claudin, Jamming, Force Chains, and Fragile Matter, Phys. Rev. Lett. 81, 1841 (1998)

[5] P. Coussot, *Rheometry of pastes, suspensions and granular materials* (Wiley, New York, 2005)

[6] D. Bonn, M.M. Denn, L. Berthier, T. Divoux, S. Manneville, Yield stress materials in soft condensed matter, Rev. Mod. Phys., 89, 035005 (2017)

[7] A. Nicolas, E.E. Ferrero, K. Martens, J.L. Barrat, Deformation and flow of amorphous solids: An updated review of mesoscale elastoplastic models, Rev. Mod. Phys. 90, 045006 (2018)

[8] P. Sollich, F. Lequeux, P. Hebraud, M.E. Cates, Rheology of Soft Glassy Materials, Phys. Rev. Lett., 78, 2020 (1997)

[9] P. Hebraud, F. Lequeux, Mode-Coupling Theory for the Pasty Rheology of Soft Glassy Materials, Phys. Rev. Lett., 81, 2934 (1998)

[10] E. Agoritsas, K. Martens, Nontrivial rheological exponents in sheared yield stress fluids, Soft Matter, 13, 4653 (2017)

[11] J. Lin, M. Wyart, Microscopic processes controlling the Herschel-Bulkley exponent, Phys. Rev. E, 97, 012603 (2018)

[12] J. Olivier, M. Renardy, On the generalization of the Hébraud–Lequeux model to multidimensional flows, Arch. Rational Mech. and Analysis, 208, 569 (2013)

[13] P. Coussot, Yield stress fluid flows: a review of experimental data, Journal of Non-Newtonian Fluid Mechanics, 211, 31 (2014)

[14] D. Doraiswamy, A.N. Mujumdar, I. Tsao, A.N. Beris, S.C. Danforth, A.B. Metzner, The Cox–Merz rule extended: a rheological model for concentrated suspensions and other materials with a yield stress, J. Rheol., 35, 647 (1991)

[15] H. Tabuteau, J.C. Baudez, P. Coussot, Flow of a yield stress fluid flowing over a rotating surface, Rheol. Acta, 46, 341 (2007)

[16] P. Saramito, A new elastoviscoplastic model based on the Herschel–Bulkley viscoplastic model, J. Non-Newtonian Fluid Mech., 158, 154 (2009)

[17] C.J. Dimitriou, R.H. Ewoldt, G.H. McKinley, Describing and prescribing the constitutive response of yield stress fluids using large amplitude oscillatory shear stress (LAOStress), J. Rheol., 57, 27 (2013)

[18] D. Fraggedakis, Y. Dimakopoulos, J. Tsamopoulos, Yielding the yield stress analysis: A thorough comparison of recently proposed elasto-visco-plastic (EVP) fluid models, J. Non-Newt. Fluid Mech., 236, 104 (2016)

[19] P. Coussot, H. Tabuteau, X. Chateau, L. Tocquer, and G. Ovarlez, Aging and solid or liquid behavior in pastes, J. Rheol., 50, 975 (2006)

[20] P. Lidon, L. Villa, S. Manneville, Power-law creep and residual stresses in a carbopol microgel, Rheol. Acta, 56, 307 (2017)

[21] V. Grenard, T. Divoux, N. Taberlet, S. Manneville, Timescales in creep and yielding of attractive gels, Soft Matter, 10, 1555-1571 (2014)

[22] G. Ovarlez and P. Coussot, The physical age of soft-jammed systems, Physical Review E 76, 011406 (2007)

[23] A. Shahin, Y.M. Joshi, Physicochemical Effects in Aging Aqueous Laponite Suspensions, Langmuir, 28, 15674 (2012)

[24] A. Shahin, Y.M. Joshi, Hyper-Aging Dynamics of Nanoclay Suspension, Langmuir, 28, 5826 (2012)

[25] A. Barbot, M. Lerbinger, A. Hernandez-Garcia, R. Garcia-Garcia, M.L. Falk, D. Vandembroucq, S. Patinet, Local yield stress statistics in model amorphous solids, Phys. Rev. E, 97, 033001 (2018)

[26] E. Lerner, I. Procaccia, Locality and nonlocality in elastoplastic responses of amorphous solids, Phys. Rev. E, 79, 066109 (2009)

[27] A. Zaccone, P. Schall, E.M. Terentjev, Microscopic origin of nonlinear nonaffine deformation in bulk metallic glasses, Phys. Rev. B, 90, 140203 (2014)

[28] J.M. van Doorn, J. Bronkhorst, R. Higler, T. van de Laar, J. Sprakel, Linking Particle Dynamics to Local Connectivity in Colloidal Gels, Phys. Rev. Lett., 118, 188001 (2017)

[29] A. Lemaitre, C. Caroli, Rate-Dependent Avalanche Size in Athermally Sheared Amorphous Solids, Phys. Rev. Lett., 103, 065501 (2009)

[30] Z. Budrikis, D. Fernandez Castellanos, S. Sandfield, M. Zaiser, S. Zapperi, Universal features of amorphous plasticity, Nature Communications, 8, 15928 (2017)

[31] A. Nicolas, J.L. Barrat, Spatial Cooperativity in Microchannel Flows of Soft Jammed Materials: A Mesoscopic Approach, Phys. Rev. Lett., 110, 138304 (2013)

[32] P. Hébraud, F. Lequeux, J.P. Munch, D.J. Pine, Yielding and rearrangements in disordered emulsions, Phys. Rev. Lett. 78, 4657 (1997)

[33] G. Petekidis, A. Moussaid, P.N. Pusey, Rearrangements in hard-sphere glasses under oscillatory shear strain, Phys. Rev. E, 66, 051402 (2002)

[34] P. Schall, D.A. Weitz, F. Spaepen, Structural Rearrangements That Govern Flow in Colloidal Glasses, Science, 318, 1895 (2007)

[35] A. Ghosh, Z. Budrikis, V. Chikkadi, A.L. Sellerio, S. Zapperi, P. Schall, Direct observation of percolation in the yielding transition of colloidal glasses, Phys. Rev. Lett., 118, 148001 (2017)

[36] K. Hyun, M. Wilhelm, C.O. Klein, K.S. Cho, J.G. Nam, K.H. Ahn, S.J. Lee, R.H. Ewoldt, G.H. McKinley, A review of nonlinear oscillatory shear tests: Analysis and application of large amplitude oscillatory shear (LAOS), Progress Polymer Sci., 36, 1697 (2011)

[40] L. Ducloué , Rheological behavior of aerated yield stress fluids, Ph.D. thesis, Univ. Paris EST (2014) (in French)

[41] P. Lidon, Effect of ultrasounds on soft materials, Ph.D. thesis, Univ. Lyon (2006) (in French)

[42] J.M. Piau, Carbopol gels: Elastoviscoplastic and slippery glasses made of individual swollen sponges: Meso- and macroscopic properties, constitutive equations and scaling laws, J. Non-Newt. Fluid Mech., 144, 1 (2007)

[43] Z.B.M Zarrouk, Study of the solid-liquid transition in a thixotropic fluid, Ph.D. thesis, Univ. Poitiers (2010) (in French)

[44] F. Pignon, A. Magnin, J.M. Piau, Butterfly Light Scattering Pattern and Rheology of a Sheared Thixotropic Clay Gel, Phys. Rev.Lett., 79, 4689 (1997)

[45] P.F. Luckham, S. Rossi, The colloidal and rheological properties of bentonite suspensions, Advances in Colloid and Interface Science,82, 43-92 (1999)

[46] H. Van Damme, P. Levitz, J.J. Fripiat, J.F. Alcover, L. Gatineau, F. Bergaya, pp. 24-30 in *Physics of Finely Divided Matter* (N. Boccara and M. Daoud, Eds., Springer Verlag, Berlin, 1985)

[47] M. Morvan, D. Espinat, J. Lambard, T. Zemb, Ultrasmall- and small-angle X-ray scattering of smectite clay suspensions, Colloids Surfaces A : Physicochem. Eng. Aspects, 82, 193 (1994)

[48] T. G. Mason, J. Bibette, D. A. Weitz, Yielding and Flow of Monodisperse Emulsions, J. Colloid Interface Sci., 179, 439-448 (1996)

[49] G. Ovarlez, S. Rodts, A. Ragouilliaux, P. Coussot, J. Goyon, A. Colin, Wide-gap Couette flows of dense emulsions: Local concentration measurements, and comparison between macroscopic and local constitutive law measurements through magnetic resonance imaging, Physical Review E 78, 036307 (2008)

[50] P. Coussot, L. Tocquer, C. Lanos, G. Ovarlez, Macroscopic vs local rheology of yield stress fluids, Journal of Non-Newtonian Fluid Mechanics, 158, 85-90 (2009)

[51] Coussot, P., Nguyen, Q.D., Huynh, H.T., and Bonn, D., Viscosity bifurcation in thixotropic, yielding fluids, *Journal of Rheology*, 46, 573-589 (2002)

[52] J.S. Raynaud, P. Moucheront, J.C. Baudez, F. Bertrand, J.P. Guilbaud, P. Coussot, Direct determination by NMR of the thixotropic and yielding behavior of suspensions, Journal of Rheology, 46, 709-732 (2002)

[53] T. Gibaud, C. Barentin, N. Taberlet, S. Manneville, Shear-induced fragmentation of laponite suspensions, Soft Matter, 5, 3026-3037 (2009)

[54] G. Ovarlez and X. Chateau, Influence of shear stress applied during flow stoppage and rest period on the mechanical properties of thixotropic suspensions, Physical Review E 77, 061403 (2008)

[55] P. Coussot, J.S. Raynaud, F. Bertrand, P. Moucheront, J.P. Guilbaud, H.T. Huynh, S. Jarny, D. Lesueur, D., Coexistence of liquid and solid phases in flowing soft-glassy materials, Physical Review Letters, 88, 218301 (2002)

[56] G. Benmouffok-Benbelkacem, F. Caton, C. Baravian, S. Skali-Lami, Nonlinear viscoelasticity and temporal behavior of typical yield stress uids: Carbopol, Xanthan and Ketchup, Rheol. Acta, 49, 305 (2010)

Appendix 1: Detailed results for the Carbopol gel and the bentonite and laponite suspensions

A.1.1 Gel

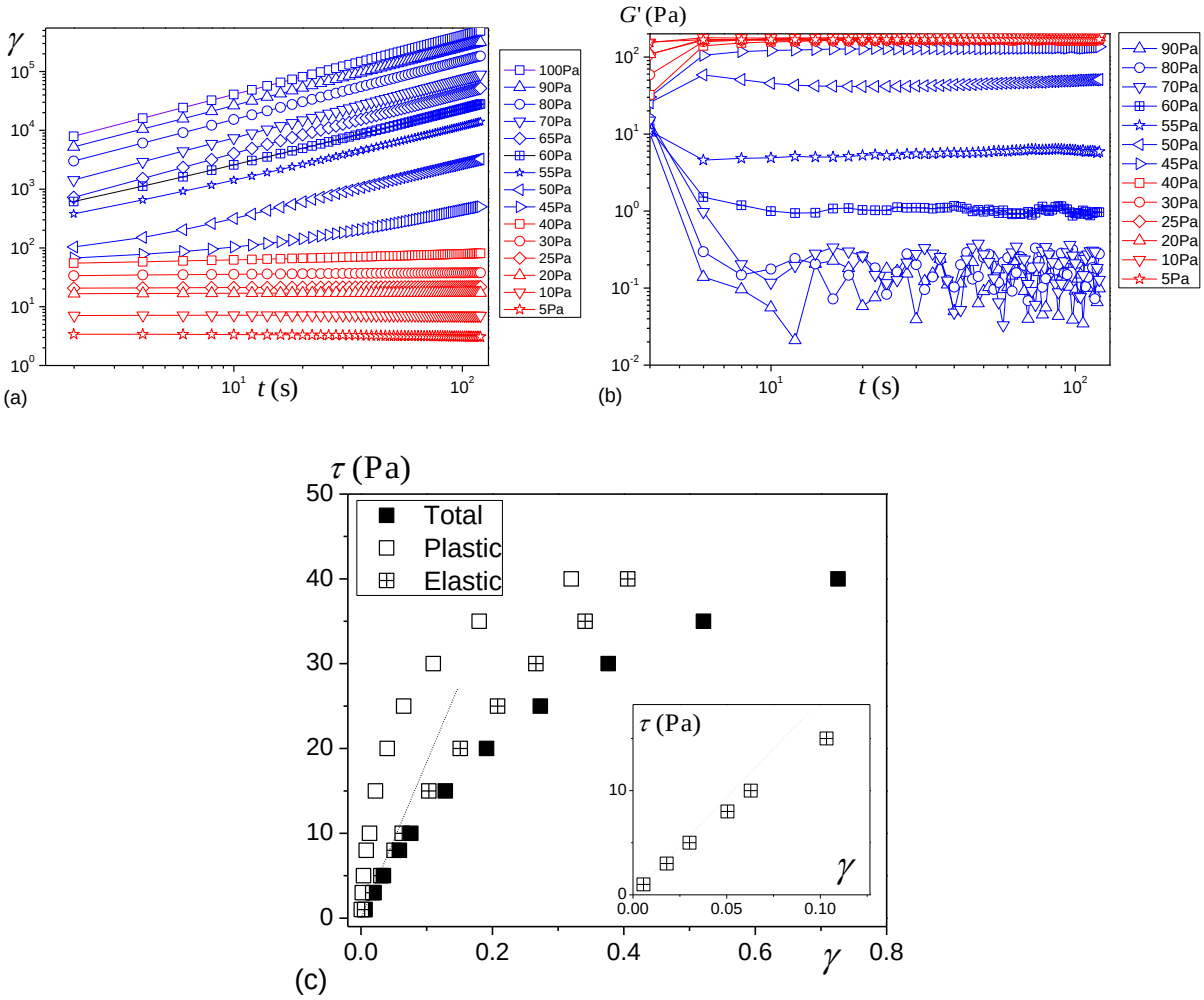

Figure A1: Gel: (a) Deformation vs time during creep tests under different stress levels; (b) Elastic modulus under low stress oscillations during creep tests; (c) Shear stress vs induced deformation during recovery tests (stress release): elastic (reversible) component, plastic (irreversible) component, total deformation. The dotted line is the equation $\tau = G_\infty \gamma$, with G_∞ taken as the constant G' (183 Pa here) in small oscillations tests. The inset shows a zoom of these data on low stress values to better appreciate the deviation of elastic deformation from linearity in that range.

A.1.2 Bentonite

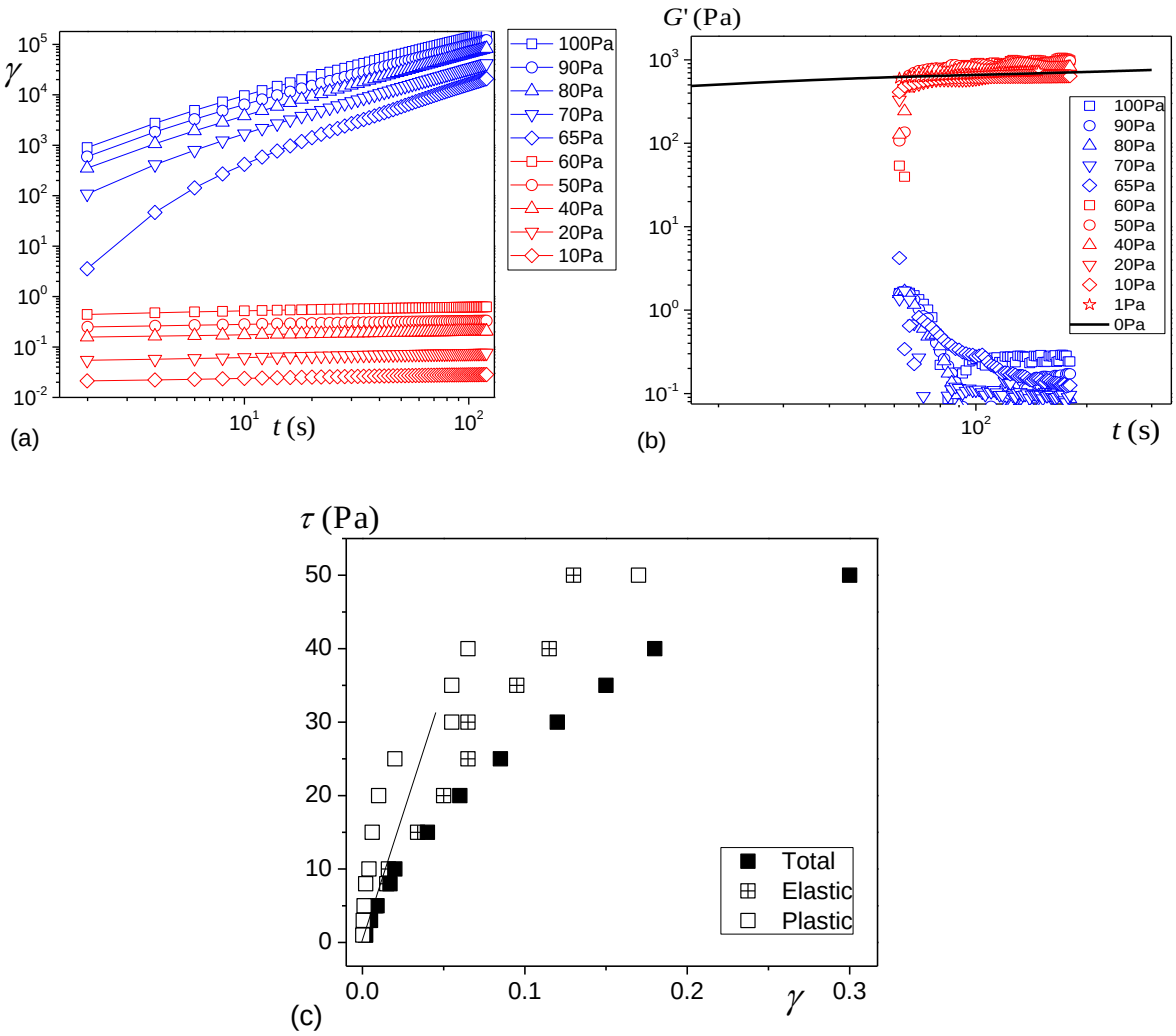

Figure A2: Bentonite suspension: (a) Deformation vs time during creep tests under different stress levels; (b) Elastic modulus under low stress oscillations during creep tests; (c) Shear stress vs induced deformation during recovery tests (stress release): elastic (reversible) component, plastic (irreversible) component, total deformation. The dotted line is the equation $\tau = G_\infty \gamma$, with G_∞ taken as the constant G' (680 Pa here) in small oscillations tests. Note that for (a) the initial time is the time at which the stress is imposed, while for (b) it is the time just after preshear.

A.1.3 Laponite

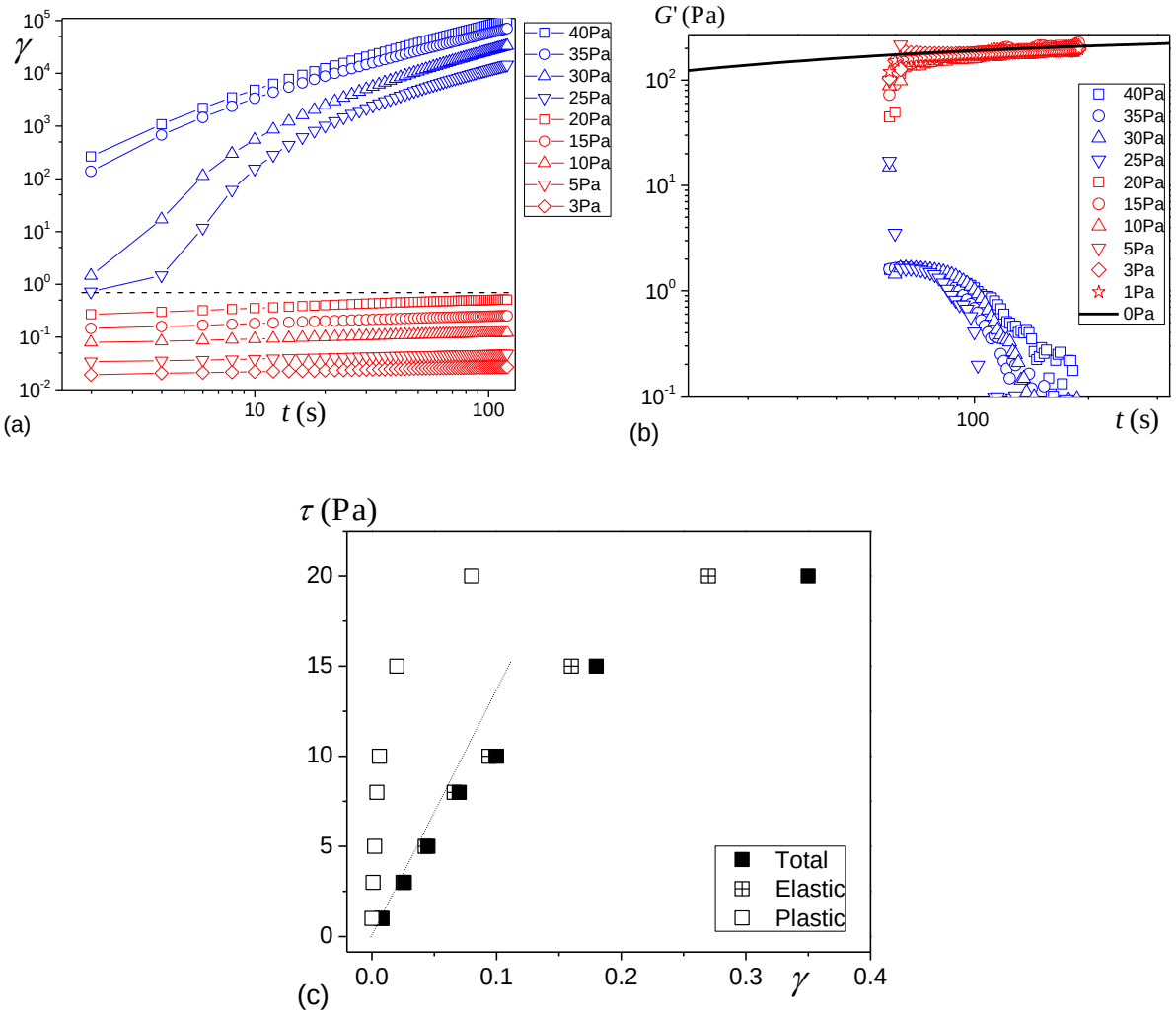

Figure A3: Laponite suspension: (a) Deformation vs time during creep tests under different stress levels; the horizontal dashed line is a guide for the eye; (b) Elastic modulus under low stress oscillations during creep tests; (c) Shear stress vs induced deformation during recovery tests (stress release): elastic (reversible) component, plastic (irreversible) component, total deformation. The dotted line is the equation $\tau = G_\infty \gamma$, with G_∞ taken as the constant G' (135 Pa here) in small oscillations tests. Note that for (a) the initial time is the time at which the stress is imposed, while for (b) it is the time just after preshear.

Appendix 2. Determination of elastic and plastic deformations.

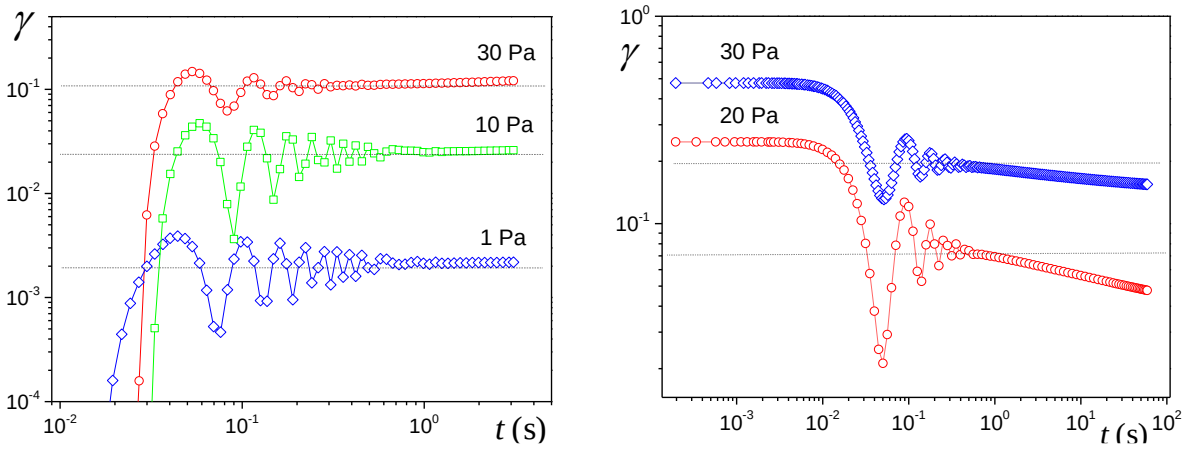

Figure A4. (a) Deformation vs time observed for creep tests on bentonite suspension at different stress levels. The horizontal dotted lines show the level of the plateau deformation retained as the measure of the elasto-plastic deformation. (b) Deformation vs time observed with Carbopol gel during recovery tests, after creep tests under different stress levels. The horizontal dotted lines show the level of the plateau deformation retained as the measure of the residual (plastic) deformation.

Appendix 3. Flow curves

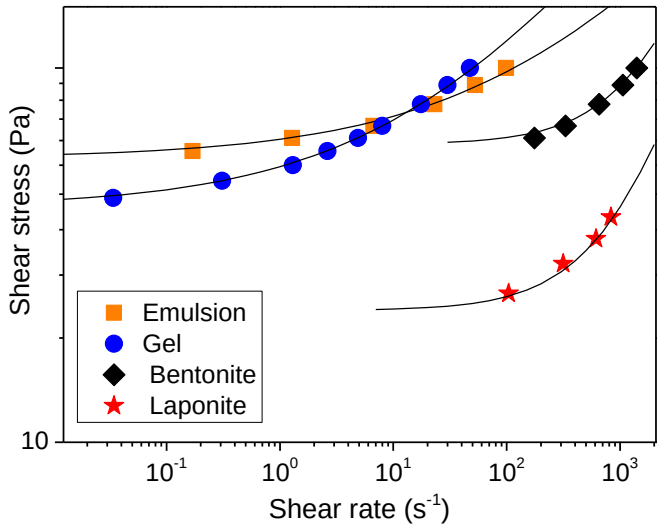

Figure A5 : Flow curve data for the different materials as deduced from steady state flows during creep tests. The continuous lines are the Herschel-Bulkley models fitted to the different material data: emulsion ($k = 7$ Pa.s^n , $n = 0.38$), gel ($k = 12$ Pa.s^n , $n = 0.4$), bentonite ($k = 0.027$ Pa.s^n , $n = 1$), laponite ($k = 0.02$ Pa.s^n , $n = 1$).